Linear momentum transfer in 292-MeV ^{20}Ne-induced fission of ^{165}Ho, ^{181}Ta, ^{197}Au, ^{209}Bi, and ^{238}U

L. E. Tubbs,* J. R. Birkelund,† and J. R. Huizenga
Departments of Chemistry and Physics and Nuclear Structure Research Laboratory, University of Rochester, Rochester, New York 14627

D. Hilscher, U. Jahnke, H. Rossner, and B. Gebauer
Hahn-Meitner-Institut für Kernforschung, 1000 Berlin 39, Federal Republic of Germany
(Received 3 December 1984)

Angular correlations of fragments both in and out of the reaction plane from 292-MeV ^{20}Ne-induced fission of ^{165}Ho, ^{181}Ta, ^{197}Au, ^{209}Bi, and ^{238}U have been measured. The correlated data have been evaluated in terms of a full linear momentum transfer component and less than full linear momentum components. The method of evaluation has also been applied to other available data for ^{16}O- and ^{20}Ne-induced reactions. The maximum angular momentum l_{FLMT} associated with full linear momentum transfer for the systems analyzed agrees with the predictions of a classical dynamical model based on the proximity nuclear potential and one-body nuclear friction. Because of projectile breakup, the angular momentum distribution in the composite nucleus is markedly distorted from the $(2l+1)$ distribution expected for full linear momentum transfer.

I. INTRODUCTION

The measurement of the fraction of the projectile momentum transferred to the composite system in a heavy ion fusionlike reaction can be made by observation of gamma-ray emission from reaction residues,[1–5] measurement of the resultant evaporation residue recoil velocity,[6–10] or by measurement of the correlation angle between fission fragments,[11–30] in the cases where fission fragments are produced in the exit channel. This paper reports on fission fragment correlation angle measurements made on the products of ^{20}Ne-induced fission of ^{165}Ho, ^{181}Ta, ^{197}Au, ^{209}Bi, and ^{238}U at a projectile bombarding energy of 292 MeV. The principal aim of the present work is to determine the cross section of events associated with complete linear momentum transfer which is assumed to be the fusion cross section. A preliminary report describing the data-analysis procedure has been published previously.[27]

II. EXPERIMENTAL PROCEDURE

A 292-MeV beam of ^{20}Ne from the VICKSI accelerator at the Hahn-Meitner-Institut was used to bombard self-supporting targets of ^{165}Ho with a thickness of 423 μg/cm^2, ^{181}Ta at 727 μg/cm^2, ^{197}Au at 400 μg/cm^2, and ^{209}Bi at 400 μg/cm^2. In addition, two 500 μg/cm^2 ^{238}U targets were used, one with a 25 μg/cm^2 carbon foil backing and the other with a 33 μg/cm^2 carbon foil backing. Kinematic coincidences between fission fragments were detected by an ion chamber with position sensitivity in the reaction plane, and a two-dimensional position sensitive avalanche counter which measured both the in-plane and out-of-plane positions of the second fragment. The angular acceptance of the ionization chamber was 16.3° in plane and ±0.95° out of plane, and the recoil detector had an in-plane acceptance angle of 24.5° and out-of-plane acceptance of 3.77° above the reaction plane and 2.83° below the reaction plane. The ion chamber was placed with its center at a scattering angle of 64.75° in the reaction plane, and the avalanche detector was placed in two positions centered at in-plane scattering angles of −98.45° and −72.85°, in order to collect spectra at all possible correlation angles. The beam position was monitored by three solid-state detectors, two placed at ±5° to the beam in the reaction plane, and a third placed at 0° in plane and 5° above the reaction plane. The detector position signals were calibrated by masks and shadow bars placed on a movable arm within the scattering chamber. Targets were set at 45° to the beam direction, and it was determined that the target rotation did not change the target position. The ion chamber position wire was 802 mm from the target and the avalanche detector position wires were 607 mm from the target. Thus, the correlation angle measurements were insensitive to small shifts in the beam spot. A schematic diagram of the scattering chamber, including the ionization counter, recoil detector, and beam monitoring detectors, is shown in Fig. 1.

The total counts in the monitor detectors were used for the normalization of the measured correlation angle spectra. Dead time corrections were obtained from a pulser signal injected into the various preamplifiers in the system, at a rate proportional to the interaction rate. Correlation angle spectra were obtained by dividing the events in the ion chamber into bins each 1.032° wide, and adding the scattering angles of the coincident nuclei detected by the ion chamber and the avalanche counter. Because of a small uncovered region in correlation angle between the two positions of the avalanche counter, some interpolation was necessary to complete the spectra. Correlation angle spectra produced in this way are integrals over the whole out-of-plane acceptance of the avalanche counter. In ad-

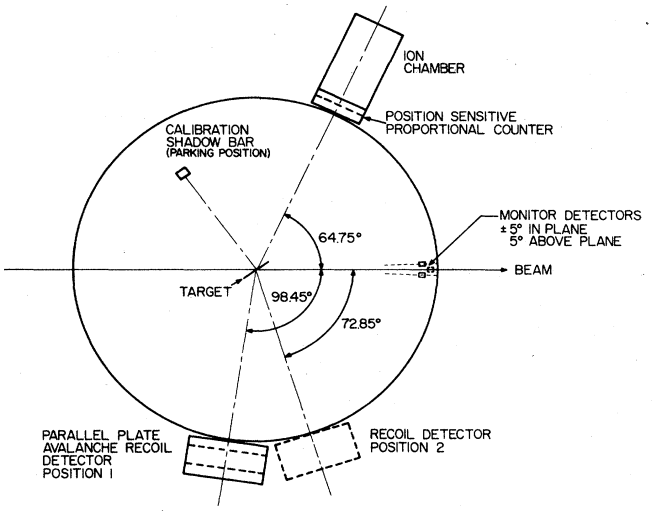

FIG. 1. Schematic drawing of scattering chamber and detectors.

dition, the out-of-plane distribution of the coincident fragments was determined by summation of the out-of-plane spectra over all measured in-plane correlation angles.

III. DATA, ANALYSES, AND RESULTS

The in-plane correlation angle spectra for coincident fragments from 292-MeV ^{20}Ne-induced fission of ^{165}Ho, ^{181}Ta, ^{197}Au, ^{209}Bi, and ^{238}U are displayed in Figs. 2–6. The arrows on the top of each figure correspond (from the left) to complete, 80%, 60%, 40%, and 20% linear momentum transfer, respectively, i.e., they signify the escape of up to four alpha particles. The angular positions of the arrows are calculated for the most probable kinetic energy release for symmetric fission. If the mass and kinetic energy distributions are folded into such calculations, the positions of the arrows shift forward[21] by approximately 0.5°. As can be seen from these figures, the angular correlation plots contain events with linear momentum transfers ranging from the initial projectile linear momentum to a small fraction of this quantity.

The present analysis of the correlation angle spectra

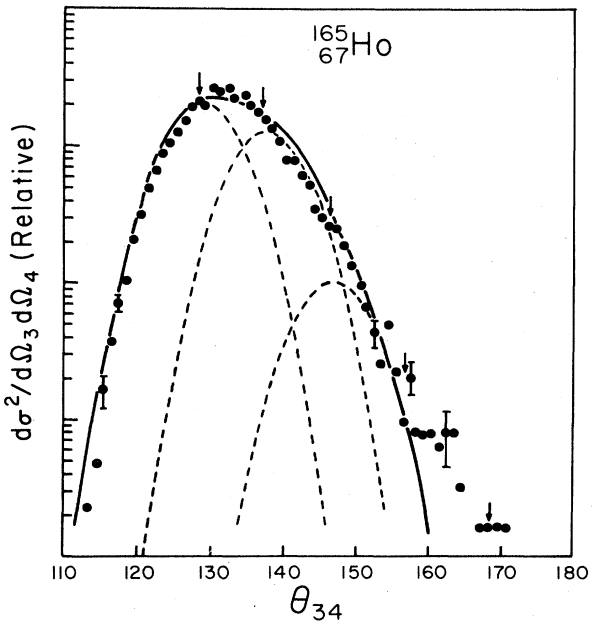

FIG. 2. In-plane correlation angle data for 292-MeV ^{20}Ne-induced fission of ^{165}Ho. The heavy line is the sum of Gaussian fits with FWHM = 10.7° to each fusion component as shown by the dashed lines.

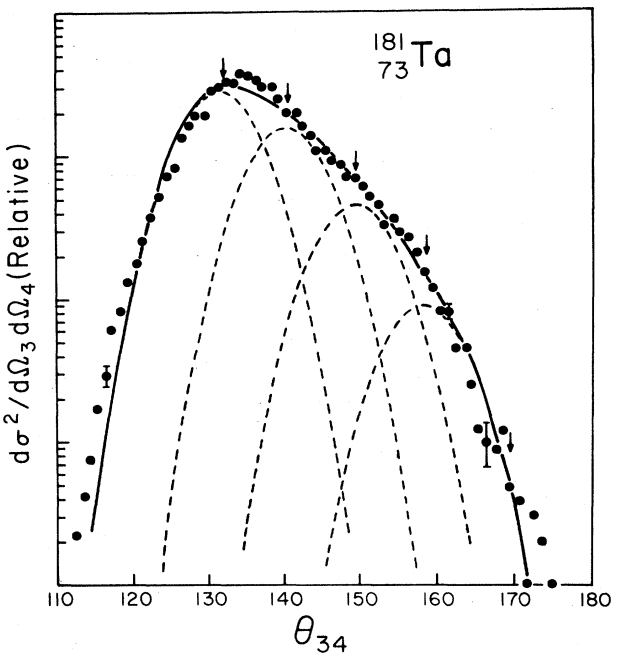

FIG. 3. Same, for a ^{181}Ta target.

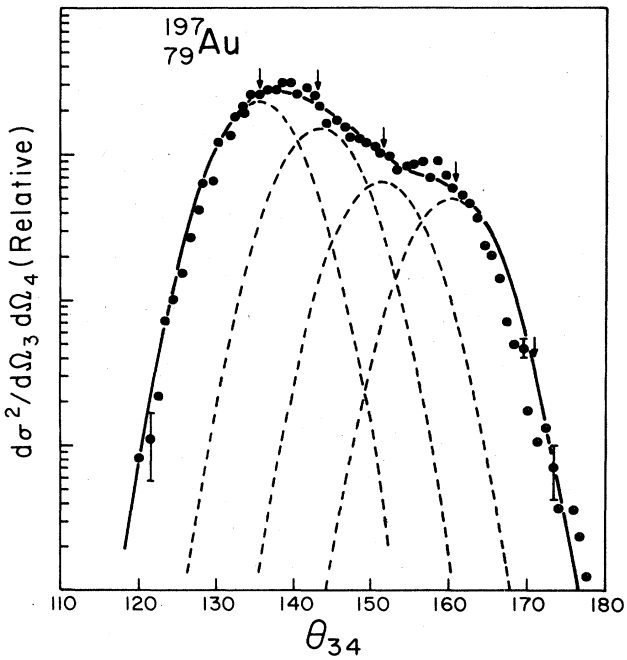

FIG. 4. Same, for a ^{197}Au target.

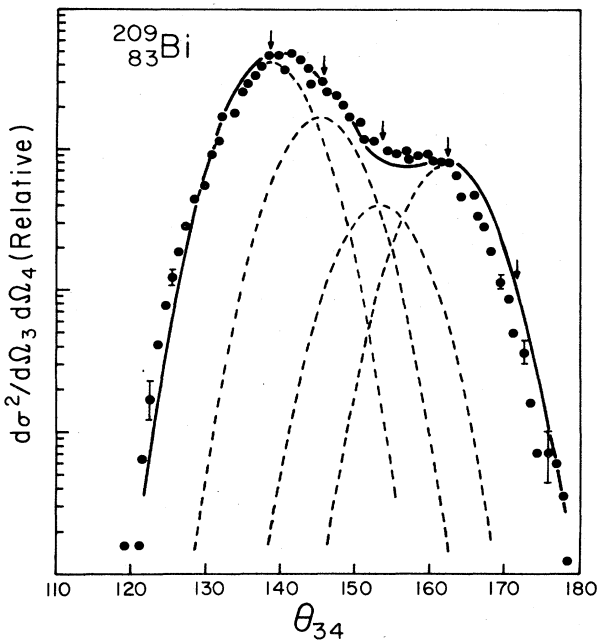

FIG. 5. Same, for a ^{209}Bi target.

makes the reasonable assumption that the measured out-of-plane dispersion in the fission fragment correlation angles is due to particle evaporation before, during, and/or after fission. Furthermore, it is assumed that particle evaporation produces a Gaussian spread of the correlation function that is symmetric in ϕ and θ about θ_{34}.

The full width at half maximum values of the Gaussian curves fitted to the out-of-plane correlation-angle spectra for coincident fission fragments of the above five targets are listed in Table I. Although the experimental full width at half maximum values (FWHM) of the out-of-plane data decrease slightly with increasing target mass, an average value of the FWHM (out of plane) of 10.7° for the five targets is consistent with the experimental errors. Furthermore, no detectable dependence of the out-of-plane FWHM on the in-plane correlation angle was observed.

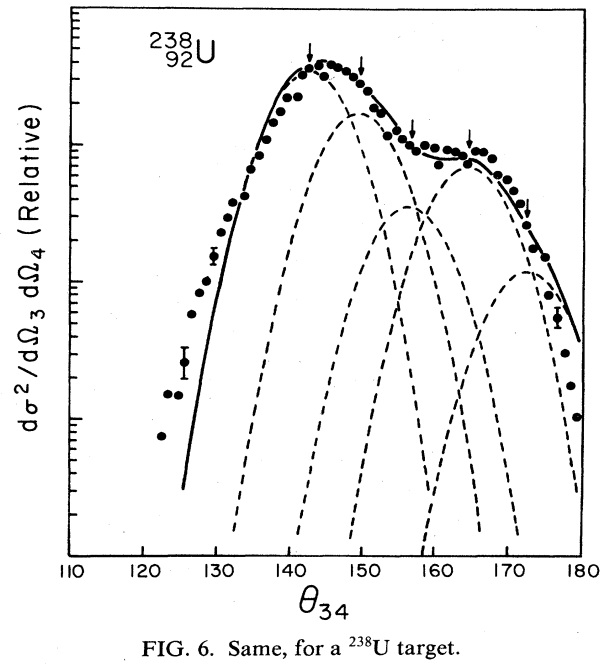

FIG. 6. Same, for a ^{238}U target.

TABLE I. Full width at half maximum values (FWHM) of the Gaussian curves fitted to the out-of-plane correlation angle spectra for coincident fissionlike fragments from 292-MeV ^{20}Ne-induced fission on the listed targets.

Target	FWHM (out-of-plane)
^{165}Ho	12.2±2 deg
^{181}Ta	11.4±2 deg
^{197}Au	10.2±2 deg
^{209}Bi	9.8±2 deg
^{238}U	9.4±2 deg

The out-of-plane FWHM values listed in Table I were used to fit each of the measured in-plane correlation angle spectra, with a series of Gaussian peaks with centroids constrained to lie at the correlation angles predicted for fission at the most probable total kinetic energy,[31] at a series of values of linear momentum corresponding to an increasing number of uncaptured alpha particles. The intensities of these various capture processes were adjusted to give the best fit to the in-plane correlation angle data. The probabilities for the various components of linear momentum transfer so derived are shown in Table II as Fit *A*. It is also possible to perform the same analysis, within the limits of experimental error, with an average value of 10.7° for the out-of-plane FWHM for the correlation angle Gaussians (Fit *B*). The resultant curves, utilizing a value of the FWHM of 10.7°, are compared to the experimental correlation angle data in Figs. 2–6. As can be seen in Table II, the derived probabilities for various components of linear momentum transfer are rather insensitive to these two assumptions about the out-of-plane widths. For the Ne projectiles considered here, the sum of the five individual linear momentum transfer components (complete, 80%, 60%, 40%, and 20%) gives a very good fit to the experimental data.

Although the alpha-particle components of linear momentum are probably the important ones for ^{20}Ne projectiles, we wish to emphasize that, in general, the subdivision of linear momentum is more complex than that employed here. However, a recent analysis[32] of our ^{197}Au + ^{20}Ne angular correlation data, including breakup fragments in addition to those with multiples of alpha particles, illustrates the importance of the alpha-particle components of linear momentum transfer for ^{20}Ne projectiles. Even so, the cross sections of the odd-Z fragments can range from one-third to one-half of those of the even-Z fragments in the secondary spectra.[35] A general procedure for extracting the distribution of linear momentum requires that the angular correlations be decomposed into a large number of Gaussians. Such a procedure was adopted by Saint-Laurent *et al.*[29] The use of such a complex subdivision of linear momentum transfer is not expected to have a significant effect on the yield of the complete linear momentum transfer component. The present

TABLE II. Probabilities of complete [$P(^{20}Ne)$], 80% [$P(^{16}O)$], 60% [$P(^{12}C)$], 40% [$P(^{8}Be)$], and 20% [$P(^{4}He)$] linear momentum transfer as deduced from fits to the experimental in-plane correlation angle spectra. Fit *A* utilizes Gaussian curves with FWHM values of Table I, whereas Fig *B* is performed with an average value of the FWHM of 10.7° for all systems. The latter value is employed in constructing the dashed and solid curves in Figs. 2—6. The values of $P(^{16}O)$, $P(^{12}C)$, $P(^{8}Be)$, and $P(^{4}He)$ are not to be equated to the yield of a single secondary fragment (10-Z, 20-A). See the text.

Target	Fit	$P(^{20}Ne)$	$P(^{16}O)$	$P(^{12}C)$	$P(^{8}Be)$	$P(^{4}He)$
^{165}Ho	*A*	0.62	0.37	0.01		
	B	0.59	0.38	0.03		
^{181}Ta	*A*	0.59	0.31	0.08	0.02	
	B	0.58	0.31	0.09	0.02	
^{197}Au	*A*	0.45	0.32	0.13	0.10	
	B	0.47	0.30	0.13	0.10	
^{209}Bi	*A*	0.57	0.26	0.07	0.10	
	B	0.59	0.24	0.06	0.11	
^{238}U	*A*	0.52	0.29	0.07	0.10	0.03
	B	0.55	0.27	0.06	0.11	0.02

TABLE III. Maximum angular momentum l_{FLMT} associated with full linear momentum transfer for ^{16}O- and ^{20}Ne-induced reactions on light and heavy targets. The quantity l_{fus}^{max} is the maximum entrance channel angular momentum for fusion as calculated with the one-dimensional potential dynamical model (Ref. 36).

Reaction	E_{lab} (MeV)	$\frac{E_{c.m.}-V_B}{\mu}$	σ_{FLMT}	Ref.	l_{FLMT}	l_{fus}^{max}	l_{FLMT}/l_{fus}^{max}
$^{27}Al+^{20}Ne$	51	0.79	710±100	a	19±2	37±1	0.51±0.06
$^{27}Al+^{20}Ne$	60	1.24	905±80	a	23±1	37±1	0.62±0.03
$^{27}Al+^{20}Ne$	81	2.27	1180±60	a	31±1	37±1	0.84±0.04
$^{27}Al+^{20}Ne$	87	2.49	1180±60	a	32±1	37±1	0.86±0.04
$^{27}Al+^{20}Ne$	93	2.89	1170±60	a	33±1	37±1	0.89±0.04
$^{27}Al+^{20}Ne$	105	3.48	1190±100	a	35±2	37±1	0.95±0.06
$^{27}Al+^{20}Ne$	120	4.24	1110±100	a	36±2	37±1	0.97±0.06
$^{27}Al+^{20}Ne$	150	5.74	890±80	a	36±2	37±1	0.97±0.06
$^{27}Al+^{20}Ne$	180	7.24	700±90	a	35±3	37±1	0.95±0.08
$^{27}Al+^{20}Ne$	290	12.74	420±110	a	35±4	37±1	0.95±0.11
$^{165}Ho+^{20}Ne$	292	9.98	1124±106	b,c,d	88±6[h]	84±2	1.05±0.08
$^{181}Ta+^{20}Ne$	292	9.69	1160±140	b,e	91±6[h]	88±2	1.03±0.07
$^{197}Au+^{20}Ne$	292	9.40	1058±116	b,f	88±5[h]	89±2	0.99±0.06
$^{209}Bi+^{20}Ne$	292	9.23	1180±140	b,e	93±6[h]	90±2	1.03±0.07
$^{235}U+^{20}Ne$	175	2.97	1350±150	g	78±4	94±2	0.83±0.05
$^{235}U+^{20}Ne$	252	6.82	1120±200	g	85±8	94±2	0.90±0.09
$^{238}U+^{16}O$	110	1.15	831±60	g	44±2	83±2	0.53±0.03
$^{238}U+^{16}O$	140	3.02	1420±120	g	65±3	83±2	0.78±0.04
$^{238}U+^{16}O$	166	4.65	1410±120	g	71±3	83±2	0.86±0.04
$^{238}U+^{16}O$	315	13.96	1150±250	g	87±10	83±2	1.05±0.12
$^{238}U+^{20}Ne$	208	4.64	1260±200	g	83±7	94±2	0.88±0.09
$^{238}U+^{20}Ne$	292	8.84	1155±140	b,e	93±6 (h)	94±2	0.99±0.07

[a]Reference 9.
[b]Table II.
[c]Reference 6.
[d]Reference 33.
[e]Reference 34.
[f]Reference 35.
[g]Reference 21.
[h]The analysis procedure may overestimate this quantity by as much as 10%.

analysis may, however, overestimate the probability of the full linear momentum component $P(^{20}\mathrm{Ne})$ by up to 20% due to an insufficient correction for mass 19 and 18 transfer.

It is important to remember that the results reported in Table II are based on the *assumption* that only α-type nuclei are captured. Hence, the magnitude of a particular $P(^{A}Z)$ is not to be understood as a measure of the yield of the single secondary fragment (10-Z, 20-A), but as the sum of yields of several nearby secondary fragments. This is especially true for components in the linear momentum spectrum with smaller linear momentum transfer, e.g., $P(^{12}\mathrm{C})$, $P(^{8}\mathrm{Be})$, and $P(^{4}\mathrm{He})$. The yields of these components, in particular, depend very strongly on the trigger angle of the fission fragments.[19] Furthermore, the conservation of cross section requires that individual P values in Table II cannot be interpreted as the yield of a single secondary fragment.

Combining the complete (or full) linear momentum transfer probability listed in Table II with a measurement of the total fission cross section gives a cross section of the full linear momentum transfer (FLMT) events σ_{FLMT} when the cross section for evaporation residues is zero. Measurements have shown that the cross section of evaporation residues is negligible[6] for the $^{197}\mathrm{Au} + {}^{20}\mathrm{Ne}$ reaction at $E_{\mathrm{lab}}=292$ MeV. Hence, the values of σ_{FLMT} for 292-MeV ^{20}Ne-induced fission of ^{181}Ta, ^{197}Au, ^{209}Bi, and ^{238}U listed in Table III are based on the assumption that the evaporation residue cross section is zero for each target. This may possibly lead to a small error in σ_{FLMT} for the $^{181}\mathrm{Ta} + {}^{20}\mathrm{Ne}$ reaction. The cross section for evaporation residues[6] with full linear momentum transfer for the $^{165}\mathrm{Ho} + {}^{20}\mathrm{Ne}$ reaction is 510 ± 50 mb. The value of σ_{FLMT} is obtained for the latter reaction by adding this value to the full linear momentum transfer component of the fission cross section.

Also included in Table III are the experimental data of Viola *et al.*[21] for the $^{235,238}\mathrm{U} + {}^{20}\mathrm{Ne}$ and $^{238}\mathrm{U} + {}^{16}\mathrm{O}$ reactions which have been subjected to the type of analysis described here. In addition, Table III includes the cross section for evaporation residues with full linear momentum transfer as a function of energy for the $^{27}\mathrm{Al} + {}^{20}\mathrm{Ne}$ reaction.[9] In the case of the latter reaction, Morgenstern *et al.*[9] have measured energy and velocity spectra and angular and mass distributions for evaporation residue products over a large range of energies. From these data it is possible to determine the fusion cross section for full linear momentum transfer, σ_{FLMT}.

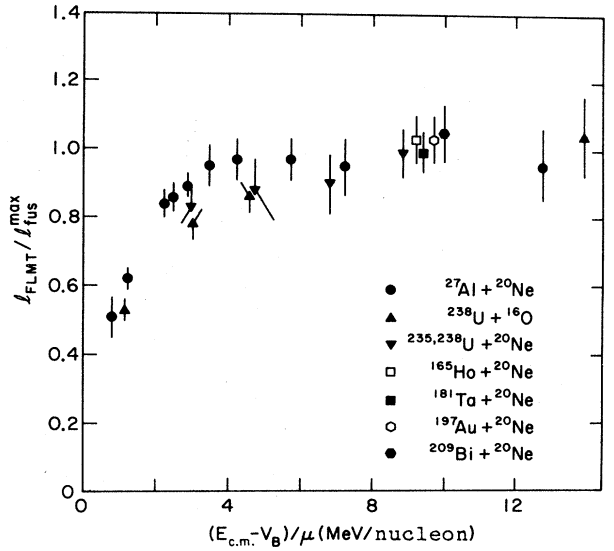

FIG. 7. Systematics of the ratio $l_{\mathrm{FLMT}}/l_{\mathrm{fus}}^{\mathrm{max}}$ as a function of $(E_{\mathrm{c.m.}}-V_B)/\mu$ in energy per nucleon. The angular momentum l_{FLMT} is the limiting angular momentum corresponding to full linear momentum transfer. The quantity $l_{\mathrm{fus}}^{\mathrm{max}}$ is the theoretical prediction of the one-dimensional classical dynamical model (Ref. 36) for the maximum angular momentum that fuses.

Assuming for simplicity a sharp cutoff model, values of l_{FLMT} are calculated from the values of σ_{FLMT} tabulated in Table III and listed in the same table. These values of l_{FLMT} implicitly assume that only the lowest angular momenta lead to full linear momentum transfer. For each reaction the maximum value of the angular momentum that fuses, $l_{\mathrm{fus}}^{\mathrm{max}}$, is calculated with a classical trajectory model[36] based on the proximity nuclear potential and one-body nuclear dissipation. These values are given in the seventh column of Table III. In Fig. 7 the ratio of the experimental maximum angular momentum for complete linear momentum fusion, l_{FLMT}, and the theoretical maximum value of the angular momentum that fuses, $l_{\mathrm{fus}}^{\mathrm{max}}$, is plotted as a function of the available energy over the barrier in MeV per nucleon $(E_{\mathrm{c.m.}}-V_B)/\mu$.

From a cursory look at Figs. 2–6, it is evident that the linear momentum transferred to the composite nucleus $P_{||}$ in 292-MeV ^{20}Ne-induced fission of heavy targets ranges from complete transfer to values considerably less than complete transfer. The most meaningful single measure

TABLE IV. Average linear momentum transfer to the composite nucleus for 292-MeV ^{20}Ne-induced fission of five heavy targets.

Fusion-fission reaction	(MeV/c)	$\langle P_{\|\|}\rangle/20$ (MeV/c)	$\dfrac{\langle P_{\|\|}\rangle}{(P_{\|\|})_{\mathrm{FLMT}}}$
$^{165}\mathrm{Ho}+{}^{20}\mathrm{Ne}$	3040	152	0.92
$^{181}\mathrm{Ta}+{}^{20}\mathrm{Ne}$	2960	148	0.89
$^{197}\mathrm{Au}+{}^{20}\mathrm{Ne}$	2740	137	0.83
$^{209}\mathrm{Bi}+{}^{20}\mathrm{Ne}$	2850	143	0.86
$^{238}\mathrm{U}+{}^{20}\mathrm{Ne}$	2770	139	0.84

of each complex correlation angle spectrum is the average linear momentum transferred to the composite nucleus $\langle P_{\|} \rangle$. In the present experiments full linear momentum transfer corresponds to a value of $\langle P_{\|} \rangle = 3311$ MeV/c. The experimental average linear momentum transferred to each target is listed in Table IV.

IV. DISCUSSION OF RESULTS

When the limiting angular momentum is plotted in terms of the ratio, $l_{\mathrm{FLMT}}/l_{\mathrm{fus}}^{\max}$, one observes that this ratio shows the same general trend for both relatively light and heavy targets when plotted against $(E_{\mathrm{c.m.}} - V_B)/\mu$. These conclusions are unaltered if the abscissa scale is changed to $[(E_{\mathrm{c.m.}} - V_B)/\mu]^{1/2}$, a quantity proportional to the relative velocity for $l = 0$. As can be seen from Fig. 7 when $(E_{\mathrm{c.m.}} - V_B)/\mu$ reaches approximately 4 MeV per nucleon, l_{FLMT} has reached its maximum value corresponding approximately to an angular momentum near the rolling limit of a collision between the target and projectile based on the proximity nuclear potential and one-body nuclear friction. The values of l_{FLMT} determined from the present data are considerably larger than those predicted by the model of Siwek-Wilczynska,[3,5] and suggest that angular momentum dissipation in the entrance channel is an important factor in determining whether fusion with full linear momentum transfer will occur.

The ratio of the cross section for full linear momentum transfer σ_{FLMT} to the cross section for capture $\sigma_{\mathrm{capture}}$ decreases as a function of increasing relative velocity. Such theoretical and experimental ratios of $\sigma_{\mathrm{FLMT}}/\sigma_{\mathrm{capture}}$ are plotted in Fig. 8 as a function of $[(E_{\mathrm{c.m.}} - V_B)/\mu]^{1/2}$ for selected light and heavy targets. Theoretical values of σ_{FLMT} are calculated with a classical dynamical model based on the proximity nuclear potential and one-body nuclear friction.[36] The values of the capture cross section are calculated by

$$\sigma_{\mathrm{capture}} = \pi R_B^2 \left[1 - \frac{V_B(R_B)}{E_{\mathrm{c.m.}}} \right] . \tag{1}$$

where R_B and $V_B(R_B)$ are determined with the nuclear proximity potential.[38] The lines in Fig. 8 represent the ratios of the two above-mentioned theoretical quantities. Although the trends in the theoretical ratios of $\sigma_{\mathrm{FLMT}}/\sigma_{\mathrm{capture}}$ are the same for all three reactions, the values of these ratios are reaction dependent when plotted as a function of $[(E_{\mathrm{c.m.}} - V_B)/\mu]^{1/2}$. The points in Fig. 8 are based on experimental values of σ_{FLMT} and either experimental or theoretical values of $\sigma_{\mathrm{capture}}$. In general, there is rather good agreement between the experimental and theoretical ratios of $\sigma_{\mathrm{FLMT}}/\sigma_{\mathrm{capture}}$. Similar conclusions have been reached also by Cassagnou *et al.*[30] in comparing data with empirical formulas[39] for complete fusion.

Morgenstern *et al.*[10] have suggested that the ratio of complete fusion to the sum of complete and incomplete fusion for composite nuclei with $A < 100$ is correlated with the velocity of the lighter nucleus v_L/c. The relationship between v_L/c and $(E_{\mathrm{c.m.}} - V_B)/\mu$, which is proportional to the relative velocity v_{rel}, is given by

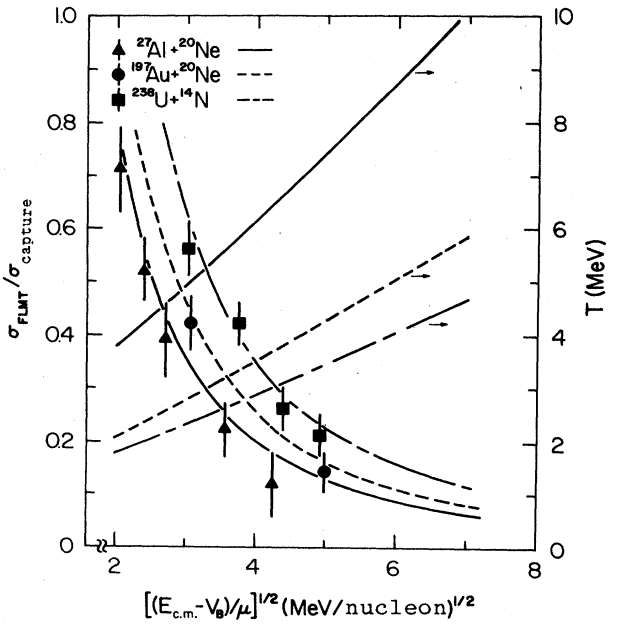

FIG. 8. Plot of the ratio $\sigma_{\mathrm{FLMT}}/\sigma_{\mathrm{capture}}$ vs $[(E_{\mathrm{c.m.}} - V_B)/\mu]^{1/2}$ for three reactions. The downward sloping lines represent theoretical ratios of $\sigma_{\mathrm{FLMT}}/\sigma_{\mathrm{capture}}$ calculated as described in the text. The experimental data are from Ref. 9 for the ^{27}Al + ^{20}Ne reaction, from Refs. 27 and 37 for the ^{197}Au + ^{20}Ne reaction, and from Ref. 28 for the ^{238}U + ^{14}N reaction. The upward sloping lines represent the temperature in MeV (right-hand ordinate) of the composite nucleus, where the temperature is defined by $T = (8E^*_{\mathrm{CN}}/A_{\mathrm{CN}})^{1/2}$.

$$\frac{v_L}{c} = 0.0463 \left[\frac{A_H}{A_H + A_L} \right] \left[\frac{E_{\mathrm{c.m.}} - V_B}{\mu} \right]^{1/2}$$

$$= \left[\frac{A_H}{A_H + A_L} \right] \frac{v_{\mathrm{rel}}}{c} , \tag{2}$$

where the units of $(E_{\mathrm{c.m.}} - V_B)/\mu$ are in MeV/nucleon. In Fig. 9 the ratio of $\sigma_{\mathrm{FLMT}}/\sigma_{\mathrm{capture}}$ is plotted versus v_L/c for the ^{27}Al + ^{20}Ne, ^{197}Au + ^{20}Ne, and ^{238}U + ^{14}N reactions. Again, as in Fig. 8, the experimental and theoretical ratios of $\sigma_{\mathrm{FLMT}}/\sigma_{\mathrm{capture}}$ show similar dependences on v_L/c for each reaction. However, both ratios are shifted to larger values of v_L/c for the heavier targets.

For fixed values of either v_L/c or v_{rel}/c, which is proportional to $[(E_{\mathrm{c.m.}} - V_B)/\mu]^{1/2}$, both the experimental and theoretical values of $\sigma_{\mathrm{FLMT}}/\sigma_{\mathrm{capture}}$ increase with increasing values of $A_H/(A_H + A_L)$. This is in contrast to results for the ratio of complete fusion to the sum of complete and incomplete fusion for composite nuclei with $A < 100$. In this case it has been shown[10] for fixed values of v_{rel}/c that the latter ratio decreases with increasing values of $A_H/(A_H + A_L)$.

When plotting data as a function of v_L/c or v_{rel}/c, as done in Figs. 8 and 9, different reactions, for the same

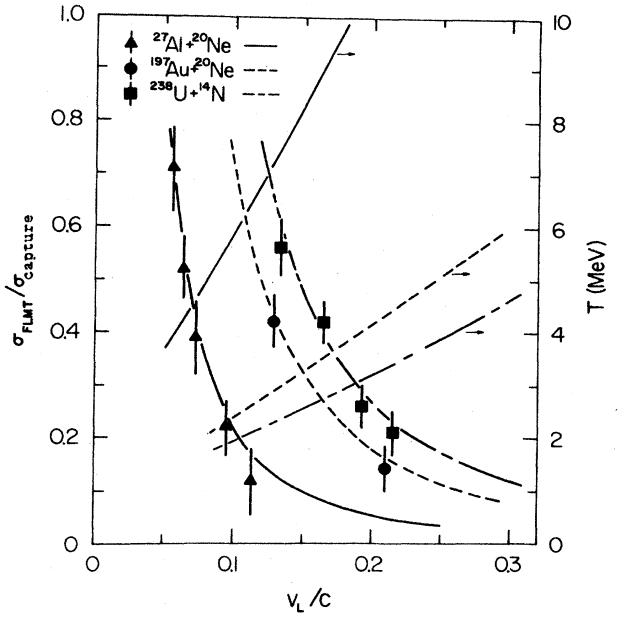

FIG. 9. Plot of the ratio $\sigma_{\mathrm{FLMT}}/\sigma_{\mathrm{capture}}$ as a function of v_L/c. See the caption of Fig. 8 and the text.

value of v/c, correspond to very different temperatures of their respective composite nuclei (CN) where the temperature is defined by $T=(8E^*_{\mathrm{CN}}/A_{\mathrm{CN}})^{1/2}$. Assuming a fixed value of $v_L/c=0.15$, for example, the temperatures of composite nuclei formed in the $^{27}\mathrm{Al}+{}^{20}\mathrm{Ne}$, $^{197}\mathrm{Au}+{}^{20}\mathrm{Ne}$, and $^{238}\mathrm{U}+{}^{14}\mathrm{N}$ reactions are 8.3, 3.2, and 2.5 MeV, respectively. The above value of v_L/c corresponds to center-of-mass energies of 386, 326, and 231 MeV, respectively. On the other hand, for a fixed value of $v_{\mathrm{rel}}/c=0.15$,

$$[(E_{\mathrm{c.m.}}-V_B)/\mu]^{1/2}=3.24\ \mathrm{MeV/nucleon}\ ,$$

the corresponding temperatures are 5.2, 2.9, and 2.5 MeV, respectively. The temperatures of the composite nuclei, corresponding to the highest energies where experimental values of $\sigma_{\mathrm{FLMT}}/\sigma_{\mathrm{capture}}$ are plotted in Figs. 8 and 9, are 6.45, 4.28, and 3.43 MeV, for the $^{27}\mathrm{Al}+{}^{20}\mathrm{Ne}$, $^{197}\mathrm{Au}+{}^{20}\mathrm{Ne}$, and $^{238}\mathrm{U}+{}^{14}\mathrm{N}$ reactions, respectively. Whereas the data for the heavy targets are measured for values of v_L/c exceeding a value of 0.2 and corresponding temperatures well below 5 MeV, such values of v_L/c for the $^{27}\mathrm{Al}+{}^{20}\mathrm{Ne}$ reaction correspond to temperatures larger than 10 MeV. The above examples illustrate that caution is required when comparing different reactions on plots of the type illustrated in Figs. 8 and 9.

The average linear momentum transfer $\langle P_{\|}\rangle$ to the composite nucleus for 292-MeV ^{20}Ne-induced fission of ^{165}Ho, ^{181}Ta, ^{197}Au, ^{209}Bi, and ^{238}U ranges from 3.04 to 2.74 GeV/c. The ratio of the average to the full linear momentum transfer, $\langle P_{\|}\rangle/(P_{\|})_{\mathrm{FLMT}}$, varies from 0.92 to 0.83. For 14.6 MeV/nucleon ^{20}Ne-induced fission of heavy targets, the above values of average linear momentum transfer are consistent with published values.[28,29]

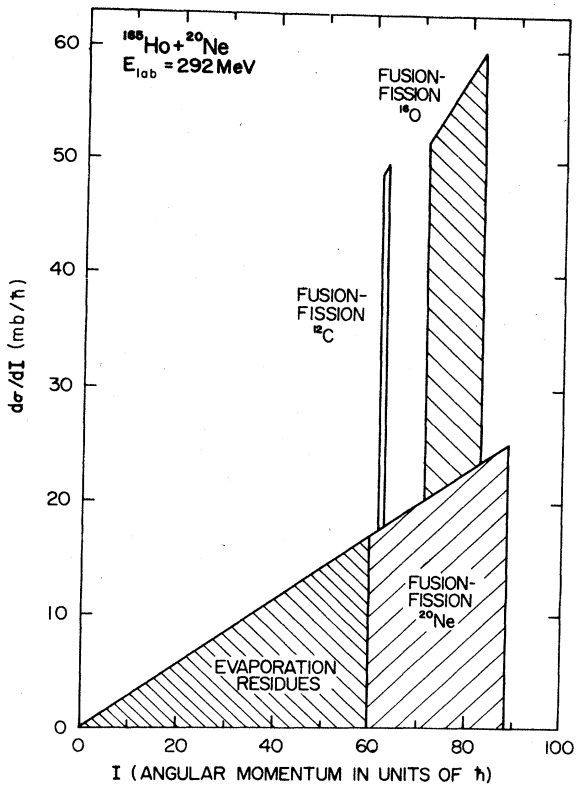

FIG. 10. Schematic plot of the differential cross section $d\sigma/dI$ as a function of angular momentum I for a system where projectile breakup occurs.

The cross section for full linear momentum transfer σ_{FLMT} for 292-MeV ^{20}Ne-induced reactions on ^{165}Ho is composed of two reaction contributions, evaporation residues and fission fragments. This is illustrated in Fig. 10 where $d\sigma/dI$, in units of mb/$\hbar$, is plotted as a function of angular momentum I. In this schematic plot it is assumed that the (full linear momentum transfer) evaporation residue cross section exhausts the lowest I values. Furthermore, a sharp cutoff model is assumed in this schematic plot. The full linear momentum transfer component of the fission cross section is distributed in I space above the evaporation residue component leading to a value of $l_{\mathrm{FLMT}}=88$. If one assumes the incomplete momentum transfer components for this reaction to be ^{16}O and ^{12}C capture with probabilities given in Table II, one obtains enhanced values of $d\sigma/dI$ in localized regions of I space as shown in Fig. 10. The actual distribution of angular momenta is expected to be much smoother than this schematic distribution calculated with the sharp cutoff approximation. However, in summary, if projectile breakup occurs leading to composite nuclei with less than full linear momentum transfer, the angular momentum in the respective composite nuclei formed with 292-MeV ^{20}Ne projectiles is markedly distorted from a $(2I+1)$ distribution expected for full linear momentum transfer.

*Present address: Department of Chemistry, Rochester Institute of Technology, Rochester, NY 14623.
†Present address: Research Laboratories, Eastman Kodak Company, 1669 Lake Ave., Rochester, NY 14650.

[1]T. Inamura *et al.*, Phys. Lett. **68B**, 51 (1977); **84B**, 71 (1979).
[2]D. R. Zolnowski *et al.*, Phys. Rev. Lett. **41**, 92 (1978).
[3]K. Siwek-Wilczynska, Phys. Rev. Lett. **42**, 1599 (1979).
[4]H. Yamada *et al.*, Phys. Rev. Lett. **43**, 605 (1979).
[5]K. Siwek-Wilczynska, Nucl. Phys. **A330**, 150 (1979).
[6]J. R. Birkelund *et al.*, Bull. Am. Phys. Soc. **26**, 539 (1981).
[7]H. Morgenstern *et al.*, Phys. Lett. **113B**, 463 (1982).
[8]Y. Chan *et al.*, Phys. Rev. C **27**, 447 (1983).
[9]H. Morgenstern *et al.*, Z. Phys. A **313**, 39 (1983).
[10]H. Morgenstern *et al.*, Phys. Rev. Lett. **52**, 1104 (1984).
[11]W. J. Nicholson and I. Halpern, Phys. Rev. **116**, 175 (1959).
[12]T. Sikkeland, E. L. Haines, and V. E. Viola, Jr., Phys. Rev. **125**, 1350 (1962).
[13]T. Sikkeland, Phys. Lett. **27B**, 277 (1968).
[14]V. E. Viola *et al.*, Nucl. Phys. **A174**, 321 (1971).
[15]H. Freiesleben, G. T. Rizzo, and J. R. Huizenga, Phys. Rev. C **12**, 42 (1975).
[16]V. E. Viola *et al.*, Nucl. Phys. **A261**, 174 (1976).
[17]T. C. Awes *et al.*, Phys. Lett. **87B**, 43 (1979).
[18]B. B. Back *et al.*, Phys. Rev. C **22**, 1927 (1980).
[19]T. C. Awes *et al.*, Phys. Rev. C **24**, 89 (1981).
[20]L. E. Tubbs, Ph.D. thesis, University of Rochester, 1982.
[21]V. E. Viola *et al.*, Phys. Rev. C **26**, 178 (1982).
[22]E. Duek *et al.*, Z. Phys. A **307**, 221 (1982).
[23]F. Saint-Laurent *et al.*, Phys. Lett. **110B**, 372 (1982).
[24]J. Galin *et al.*, Phys. Rev. Lett. **48**, 1787 (1982).
[25]U. Lynen *et al.*, Nucl. Phys. **A387**, 129c (1982).
[26]M. F. Rivet *et al.*, Nucl. Phys. **A387**, 143c (1982).
[27]J. R. Huizenga *et al.*, Phys. Rev. C **28**, 1853 (1983).
[28]M. B. Tsang *et al.*, Phys. Lett. **134B**, 169 (1984).
[29]F. Saint-Laurent *et al.*, Nucl. Phys. **A422**, 307 (1984).
[30]Y. Cassagnou *et al.*, Proceedings of the INS-RIKEN International Symposium on Heavy Ion Physics, J. Phys. Soc. Jpn. Suppl. **54**, 422 (1985).
[31]V. E. Viola, Jr., Nucl. Data **A1**, 391 (1966).
[32]B. G. Harvey and H. Homeyer, report, 1984.
[33]E. Holub, D. Hilscher, U. Jahnke, H. Orf, H. Rossner, and G. Ingold, in *Proceedings of the 3rd International Conference on Nuclear Reaction Mechanisms, Varenna, 1982,* edited by E. Gadioli (University of Milano, Milano, 1982).
[34]U. Jahnke, private communication. These fusion cross sections were deduced from neutron multiplicity measurements which show a very broad peak at large neutron multiplicity. This component was identified with fission, however, does not include fission processes associated with small neutron multiplicity. An estimate of this uncertainty is included in the assigned errors.
[35]Ch. Egelhaaf *et al.*, Hahn-Meitner-Institut Report 83/4R, 1983.
[36]J. R. Birkelund, L. E. Tubbs, J. R. Huizenga, J. N. De, and D. Sperber, Phys. Rep. **56**, 107 (1979).
[37]G. Nebbia *et al.*, Z. Phys. A **311**, 247 (1983).
[38]J. R. Birkelund and J. R. Huizenga, Annu. Rev. Nucl. Part. Sci. **33**, 265 (1983).
[39]W. W. Wilcke *et al.*, At. Data Nuclear Data Tables **25**, 389 (1980).